Poloidal Magnetic Flux Profile Control in Tokamaks via Normalized Coprime Factorization Robust Control

Justin Barton, Yongsheng Ou, Chao Xu, Eugenio Schuster and Michael Walker

Abstract— **The potential steady-state operation of a fusion tokamak, with good confinement and a high fusion gain, is related to setting up a suitable current density profile in the device. Experiments at the DIII-D tokamak focus on creating the desired current profile during the plasma current ramp-up and early flat-top phases of the discharge with the aim of maintaining this target profile throughout the subsequent phases of the discharge. The time evolution of the current density profile in a tokamak is related to the time evolution of the poloidal magnetic flux profile, which is modeled in normalized cylindrical coordinates by a partial differential equation referred to as the magnetic diffusion equation. Extremum seeking and nonlinear programming techniques have been employed to find optimal open-loop (feedforward) solutions to the finite time control problem during the ramp-up and early flat-top phases. In order to reject the effects of external disturbances to the system, we propose an optimal H_∞ feedback control input that is added to the optimal feedforward control input to regulate the poloidal flux profile around the desired reference trajectories of the system. The combined feedforward + feedback, model-based controller is then tested through simulation.**

I. Introduction

Nuclear fusion is the process by which two light nuclei "fuse" together to form one heavier nucleus, and the mass lost in the reaction is converted into energy. In order for the fusion reaction to occur frequently, the nuclei must be heated to temperatures of about one million degrees Celsius. At these temperatures, the reactants are in the plasma state. One of the most promising devices capable of achieving controlled nuclear fusion is the tokamak, which confines the plasma by using magnetic fields. The ITER project is attempting to prove the technical feasibility of a commercial nuclear fusion power plant. However, in order for the ITER project to be successful, there are several challenging control problems that still need to be solved.

One such challenge is the capability to operate the tokamak for "steady state" plasma discharges in which the plasma current will have to be generated by non-inductive means. One advanced tokamak operating scenario, characterized by non-inductive sustainment of the plasma current, is related to setting up a suitable current density profile in the device. Advances in current profile control at the JET tokamak can be found in [1], [2], [3]. Also, profile control at the Tore Supra and JT-60U tokamaks is discussed in [4], [5], [6]. Progress towards control-oriented modeling of the current profile is explored in [7], [8].

One method of current profile control, and the one employed at the DIII-D tokamak, is to create the desired current profile during the ramp-up and early flat-top phases of the total plasma current pulse, and then to actively maintain this profile throughout the subsequent phases of the discharge. Active feedback control of the evolution of the current profile at discrete points in the tokamak has been tested at DIII-D [9]. The employed controller requests a power level to the actuator, either electron cyclotron heating (ECH) or neutral beam injection (NBI), that is equal to a preprogrammed feedforward value plus the error times a proportional gain. Some present limitations of this non-model-based, proportional controller, such as oscillations and instability under certain operating conditions, motivate the design of a model-based controller that takes into account the dynamics of the whole current profile in response to the different actuators and has the potential for improved performance.

The time evolution of the current profile is related to the time evolution of the poloidal magnetic flux profile, which is modeled in normalized cylindrical coordinates by a partial differential equation (PDE) referred to as the magnetic flux diffusion equation. A control-oriented model of the current profile time evolution, valid in the ramp-up and early flat-top phases of the discharge, was developed in [8]. The actuators used to achieve the desired current profile are physically constrained in magnitude as well as in rate of change, and as a result, experiments have shown that some of the desired current profiles may not be achievable for all arbitrary initial conditions. Therefore, the objective becomes to achieve the best possible matching during the ramp-up and early flat-top phases of the plasma current pulse, which can be treated as a finite-time optimal control problem for a nonlinear PDE system. Nonlinear programming [10] and extremum seeking [11] were used to design optimal open-loop (feedforward) algorithms for this control problem. In order to reject the effects of external disturbances to the system, a feedback control input is added to the optimal feedforward control input to regulate the poloidal flux profile around the desired reference trajectories of the system. In this work, we design a robust feedback control algorithm to accomplish these goals.

This paper is organized as follows. In section II, we introduce an infinite dimensional model for the poloidal magnetic

This work was supported by the NSF CAREER award program (ECCS-0645086) and the U.S. Department of Energy (DE-FG02-09ER55064, DE-FG02-92ER54141 and DE-FC02-04ER54698). J. Barton (justin.barton@lehigh.edu) and E. Schuster are with the Department of Mechanical Engineering and Mechanics, Lehigh University, 19 Memorial Drive West, Bethlehem, PA 18015, USA. Y. Ou is with the Center for Intelligent and Biomimetic Systems, Shenzhen Institute of Advanced Technology, Shenzhen, China. C. Xu is with the Institute of Cyber-Systems and Control, Department of Control Science and Engineering, Zhejiang University, Hangzhou, China. M. Walker is with General Atomics, 3550 General Atomics Court, San Diego, CA 92121, USA.

flux. The governing PDE is reduced to a finite dimensional system of ordinary differential equations (ODEs) by employing a truncated Taylor series expansion in space, and a linear, time varying state-space representation of the tracking error is derived in section III. In section IV, the time varying state-space system is represented as an uncertain state-space model and formulated into a robust control framework. An optimal H_∞ feedback controller, based on the normalized coprime factorization technique, is designed in section V, and the combined feedforward + feedback controller is tested through simulation in section VI. Conclusions and future work are presented in section VII.

II. Current Profile Evolution Model

Any arbitrary quantity that is constant on each magnetic surface within the tokamak plasma can be used to index the magnetic surfaces. We choose as the indexing variable the mean geometric minor radius, ρ, of the magnetic surface, i.e., $\pi B_{\phi,0}\rho^2 = \Phi$, where Φ is the toroidal magnetic flux and $B_{\phi,0}$ is the reference magnetic field at the geometric major radius R_0 of the tokamak. The variable $\hat{\rho}$ is used to denote the normalized minor radius ($\hat{\rho} = \rho/\rho_b$) where ρ_b is the minor radius of the last closed magnetic flux surface. During the ramp-up and early flat-top phases of the tokamak discharge, the plasma current is mainly driven by induction. Based on experimental observations at DIII-D, simplified scenario-oriented models for the electron temperature, the non-inductive current density, and the plasma resistivity were identified [8]. By using these simplified models, the evolution of the poloidal magnetic flux in normalized cylindrical coordinates is given by the magnetic diffusion equation

$$\frac{\partial \psi}{\partial t} = f_1(\hat{\rho})u_1(t)\frac{1}{\hat{\rho}}\frac{\partial}{\partial \hat{\rho}}\left(\hat{\rho} f_4(\hat{\rho})\frac{\partial \psi}{\partial \hat{\rho}}\right) + f_2(\hat{\rho})u_2(t) \quad (1)$$

with boundary conditions

$$\left.\frac{\partial \psi}{\partial \hat{\rho}}\right|_{\hat{\rho}=0} = 0 \qquad \left.\frac{\partial \psi}{\partial \hat{\rho}}\right|_{\hat{\rho}=1} = -k_3 u_3(t) \quad (2)$$

where ψ is the poloidal magnetic flux, t is the time, $f_1(\hat{\rho})$, $f_2(\hat{\rho})$, and $f_4(\hat{\rho})$ are functions of the simplified models, k_3 is a constant, and

$$u_1(t) = \left(\frac{\bar{n}(t)}{I(t)\sqrt{P_{tot}(t)}}\right)^{3/2} \quad u_2(t) = \frac{\sqrt{P_{tot}(t)}}{I(t)} \quad u_3(t) = I(t) \quad (3)$$

where $I(t)$ denotes the total plasma current, $P_{tot}(t)$ denotes the total power of the non-inductive sources of current (NBI, ECH, etc.), and $\bar{n}(t)$ denotes the line averaged plasma density [8]. The control actuators for the ramp-up and early flat-top phases of the discharge are $I(t)$, $P_{tot}(t)$, and $\bar{n}(t)$. It is important to note that the waveforms generated by the controller proposed in this work represent the references to the respective physical controllers.

III. Model Reduction Via Truncated Taylor Series Expansion

To construct a reduced-order model suitable for control design, the governing PDE is discretized in space using a truncated Taylor series expansion to approximate the spatial derivatives while leaving the time domain continuous [12]. The non-dimensional domain of interest, [0,1], is represented as l nodes, and the spacing between the nodes, $\Delta\hat{\rho}$, is defined as $\Delta\hat{\rho} = 1/(l-1)$. In order to discretize the magnetic diffusion equation, (1) is expanded using the chain rule as

$$\frac{\partial \psi}{\partial t} = f_1 u_1(t)\frac{1}{\hat{\rho}}\left[\hat{\rho}\frac{\partial \psi}{\partial \hat{\rho}}\frac{df_4}{d\hat{\rho}} + f_4\frac{\partial \psi}{\partial \hat{\rho}} + \hat{\rho} f_4\frac{\partial^2 \psi}{\partial \hat{\rho}^2}\right] + f_2 u_2(t). \quad (4)$$

Central finite difference spatial derivative approximations of $O(\Delta\hat{\rho}^2)$ are used in the interior node region, $2 \le i \le (l-1)$. For the boundary node, $i = 1$, forward finite difference spatial derivative approximations of $O(\Delta\hat{\rho}^2)$ are used, and backward finite difference spatial derivative approximations of $O(\Delta\hat{\rho}^2)$ are used for the boundary node, $i = l$.

After applying the spatial derivative approximations to (4) and taking into account the boundary conditions (2), we obtain a matrix representation for the reduced-order model

$$\dot{\alpha}(t) = M\alpha(t)v_1(t) + Nv_2(t) + Zv_3(t). \quad (5)$$

The vector $[v_1(t), v_2(t), v_3(t)]^T = [u_1(t), u_2(t), u_1(t)u_3(t)]^T \in \mathbb{R}^{3\times 1}$ is the control input, the vector $\alpha = [\psi_1, \ldots, \psi_l]^T \in \mathbb{R}^{l\times 1}$ is the value of $\psi(\hat{\rho}, t)$ at the l nodes, and $M \in \mathbb{R}^{l\times l}$, $N \in \mathbb{R}^{l\times 1}$, and $Z \in \mathbb{R}^{l\times 1}$ are the system matrices. The system matrices for the boundary node $i = 1$ are defined as

$$M_{1,j} = f_1(0)f_4(0)\left(\frac{a_j}{4(\Delta\hat{\rho}^2)}\right) \quad N_1 = f_2(0) \quad Z_1 = 0 \quad (6)$$

where $j = 1, \ldots, 4$, $a_1 = -4$, $a_2 = 1$, $a_3 = 4$, and $a_4 = -1$. The system matrices for the interior node region, $2 \le i \le (l-1)$, are defined as

$$\begin{aligned} M_{i,i-1} &= \frac{f_1(\Delta x)}{\Delta x}\left[f_4(\Delta x)\left(\frac{-1}{2\Delta\hat{\rho}}\right) + \Delta x f_4(\Delta x)\left(\frac{1}{\Delta\hat{\rho}^2}\right)\right. \\ &\quad \left. + \Delta x\left(\frac{-1}{2\Delta\hat{\rho}}\right)\left(\frac{df_4(\Delta x)}{d\hat{\rho}}\right)\right] \\ M_{i,i} &= f_1(\Delta x)f_4(\Delta x)\left(\frac{-2}{\Delta\hat{\rho}^2}\right) \\ M_{i,i+1} &= \frac{f_1(\Delta x)}{\Delta x}\left[f_4(\Delta x)\left(\frac{1}{2\Delta\hat{\rho}}\right) + \Delta x f_4(\Delta x)\left(\frac{1}{\Delta\hat{\rho}^2}\right)\right. \\ &\quad \left. + \Delta x\left(\frac{1}{2\Delta\hat{\rho}}\right)\left(\frac{df_4(\Delta x)}{d\hat{\rho}}\right)\right] \\ N_i &= f_2(\Delta x) \quad Z_i = 0 \end{aligned} \quad (7)$$

where $\Delta x = (i-1)\Delta\hat{\rho}$. The system matrices for the boundary node $i = l$ are defined as

$$\begin{aligned} M_{l,j} &= f_1(1)f_4(1)\left(\frac{b_j}{-4(\Delta\hat{\rho}^2)}\right) \quad N_l = f_2(1) \\ Z_l &= -k_3 f_1(1)\left[f_4(1) + f_4(1)\left(\frac{-3}{-2\Delta\hat{\rho}}\right) + \frac{df_4(1)}{d\hat{\rho}}\right] \end{aligned} \quad (8)$$

where $j = l-3, \ldots, l$, $b_{l-3} = 1$, $b_{l-2} = -4$, $b_{l-1} = -1$ and $b_l = 4$. All other entries in the M system matrix are zero.

Let $\alpha_{FF}(t)$ and $v_{FF}(t)$ be the optimal open-loop (feedforward) trajectories of the states and control inputs respectively with initial condition $\alpha_{FF}(0)$. These trajectories satisfy

$$\dot{\alpha}_{FF}(t) = M\alpha_{FF}(t)v_{1_{FF}}(t) + Nv_{2_{FF}}(t) + Zv_{3_{FF}}(t). \quad (9)$$

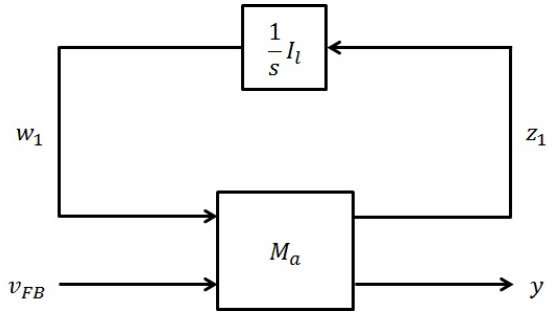

Fig. 1. Transfer function $G(s)$ represented as a LFT.

Defining the fluctuation variables $e(t) = \alpha(t) - \alpha_{FF}(t)$ and $v_{FB}(t) = v(t) - v_{FF}(t)$, where $e(t)$ is the tracking error and $v_{FB}(t)$ is the feedback controller, inserting them into (5), and neglecting the nonlinear dynamics results in a linear, time variant state-space dynamic model for the error $e(t)$

$$\begin{aligned} \dot{e}(t) &= A(t)e(t) + B(t)v_{FB}(t) \\ y(t) &= Ce(t) + Dv_{FB}(t) \end{aligned} \tag{10}$$

where $A(t) = Mv_{1_{FF}}(t) \in \mathbb{R}^{l\times l}$, $B(t) = [M\alpha_{FF}(t), N, Z] \in \mathbb{R}^{l\times 3}$, $C = I_l$ is an $l \times l$ identity matrix, $D = 0$, and $v_{FB}(t) = [v_{1_{FB}}(t), v_{2_{FB}}(t), v_{3_{FB}}(t)]^T \in \mathbb{R}^{3\times 1}$. Here $\alpha(t)$, and therefore $e(t)$, is assumed measurable.

IV. Model in Robust Control Framework

A linear system with state-space matrices A, B, C, and D has a transfer function representation $G(s) = C(sI_l - A)^{-1}B + D$, where l is the number of states of the system and s denotes the Laplace variable. By defining the matrix

$$M_a = \begin{bmatrix} A & B \\ C & D \end{bmatrix}, \tag{11}$$

the system transfer function $G(s)$ can be written as a linear fractional transformation (LFT) as

$$\begin{aligned} G(s) &= F_u\left(M_a, \frac{1}{s}I_l\right) = M_{a_{22}} + M_{a_{21}}\frac{1}{s}I_l\left(I_l - M_{a_{11}}\frac{1}{s}I_l\right)^{-1}M_{a_{12}} \\ &= D + C\frac{1}{s}I_l\left(I_l - A\frac{1}{s}I_l\right)^{-1}B = D + C(sI_l - A)^{-1}B \end{aligned} \tag{12}$$

where F_u denotes the upper LFT. The block diagram of the system transfer function $G(s)$ is shown in Figure 1.

The time varying parameters $v_{1_{FF}}(t)$ and $\alpha_{FF}(t)$ in the definition of the system matrices of (10) are chosen to be modeled as a time varying uncertainty as

$$v_{1_{FF}}(t) = \gamma_v\left(1 + \beta_v\delta_v(t)\right) \qquad \alpha_{i_{FF}}(t) = \gamma_\alpha^i\left(1 + \beta_\alpha^i\delta_\alpha^i(t)\right) \tag{13}$$

where $\gamma_v = (v_{1_{FF_{max}}} + v_{1_{FF_{min}}})/2$, $\gamma_\alpha^i = (\alpha_{i_{FF_{max}}} + \alpha_{i_{FF_{min}}})/2$, $\beta_v = (v_{1_{FF_{max}}} - v_{1_{FF_{min}}})/(2\gamma_v)$, and $\beta_\alpha^i = (\alpha_{i_{FF_{max}}} - \alpha_{i_{FF_{min}}})/(2\gamma_\alpha^i)$ with $|\delta_v(t)| \leq 1$ and $|\delta_\alpha^i(t)| \leq 1$ where $i = 1, 2, \ldots, l$. By employing (13), the model for the error dynamics (10) is expressed as

$$\dot{e}_k = \sum_{j=1}^{l}\left[A_{0_{k,j}} + \delta_v(t)A_{1_{k,j}}\right]e_j + \left[B_{0_k} + \sum_{i=1}^{l}\delta_\alpha^i(t)B_{i_k}\right]v_{FB} \tag{14}$$

where

$$A_{0_{k,j}} = \gamma_v M_{k,j} \qquad A_{1_{k,j}} = \gamma_v\beta_v M_{k,j}$$

$$B_{0_k} = \left[\sum_{i=1}^{l}\gamma_\alpha^i M_{k,i}, N_k, Z_k\right] \qquad B_{i_k} = \left[(\gamma_\alpha^i\beta_\alpha^i)M_{k,i}, 0, 0\right] \tag{15}$$

and $k = 1, 2, \ldots, l$, e_k denotes the k-th component of e, $A_{0_{k,j}}$ and $A_{1_{k,j}}$ denote the k-th row j-th column component of A_0 and A_1 respectively, B_{0_k} and B_{i_k} denote the k-th component of B_0 and B_i respectively, $M_{k,i}$ denotes the k-th row i-th column component of M, and N_k and Z_k denote the k-th component of N and Z respectively. By defining the total uncertainty vector δ as $\delta = [\delta_v, \delta_\alpha^1, \ldots, \delta_\alpha^l] \in \mathbb{R}^{l+1}$, the matrix M_a, defined in (11), is written as a general affine state-space uncertainty

$$M_a = \begin{bmatrix} A_0 + \sum_{n=1}^{l+1}\delta_n(t)A_n^* & B_0 + \sum_{n=1}^{l+1}\delta_n(t)B_n^* \\ C_0 + \sum_{n=1}^{l+1}\delta_n(t)C_n^* & D_0 + \sum_{n=1}^{l+1}\delta_n(t)D_n^* \end{bmatrix} \tag{16}$$

where A_0 and B_0 are defined in (15), δ_n denotes the n-th component of δ, and

$$\begin{aligned} &A_1^* = A_1 \qquad A_{2,3,\ldots,l+1}^* = 0 \\ &B_1^* = 0 \qquad B_{2,3,\ldots,l+1}^* = B_{1,2,\ldots,l} \\ &C_0 = I_l \qquad C_{1,2,\ldots,l+1}^* = 0 \qquad D_0 = 0 \qquad D_{1,2,\ldots,l+1}^* = 0. \end{aligned} \tag{17}$$

By exploiting the structure of the state matrices in (16), the uncertainty is formulated into a LFT by achieving the smallest possible number of repeated blocks by employing the method outlined in [13]. With this purpose in mind, the matrix J_n is formed as

$$J_n = \begin{bmatrix} A_n^* & B_n^* \\ C_n^* & D_n^* \end{bmatrix} \in \mathbb{R}^{2l\times l+3}. \tag{18}$$

By using singular value decomposition and grouping terms, the matrix J_n is expressed as

$$J_n = U_n\Sigma_n V_n^* = (U_n\sqrt{\Sigma_n})(\sqrt{\Sigma_n}V_n^*) = \begin{bmatrix} L_n \\ W_n \end{bmatrix}\begin{bmatrix} R_n \\ Z_n \end{bmatrix}^* \tag{19}$$

where $[\cdot]^*$ denotes the complex conjugate transpose. If the rank of the matrix J_n is q_n, then each inner matrix has the dimensions $L_n \in \mathbb{R}^{l\times q_n}$, $W_n \in \mathbb{R}^{l\times q_n}$, $R_n \in \mathbb{R}^{l\times q_n}$, and $Z_n \in \mathbb{R}^{3\times q_n}$. By employing (19), the uncertainty is written as

$$\delta_n(t)J_n = \begin{bmatrix} L_n \\ W_n \end{bmatrix}[\delta_n(t)I_{q_n}]\begin{bmatrix} R_n \\ Z_n \end{bmatrix}^* \tag{20}$$

and the matrix M_a, defined in (16), is finally expressed as

$$M_a = \begin{bmatrix} A_0 & B_0 \\ C_0 & D_0 \end{bmatrix} + \sum_{n=1}^{l+1}\delta_n(t)J_n = Q_{11} + Q_{12}\Delta Q_{21} \tag{21}$$

where

$$Q_{11} = \begin{bmatrix} A_0 & B_0 \\ C_0 & D_0 \end{bmatrix} \quad Q_{12} = \begin{bmatrix} L_1 & \ldots & L_{l+1} \\ W_1 & \ldots & W_{l+1} \end{bmatrix}$$

$$Q_{21} = \begin{bmatrix} R_1^* & Z_1^* \\ \vdots & \vdots \\ R_{l+1}^* & Z_{l+1}^* \end{bmatrix} \quad \Delta = \begin{bmatrix} \delta_1 I_{q_1} & & 0 \\ & \ddots & \\ 0 & & \delta_{l+1}I_{q_{l+1}} \end{bmatrix}. \tag{22}$$

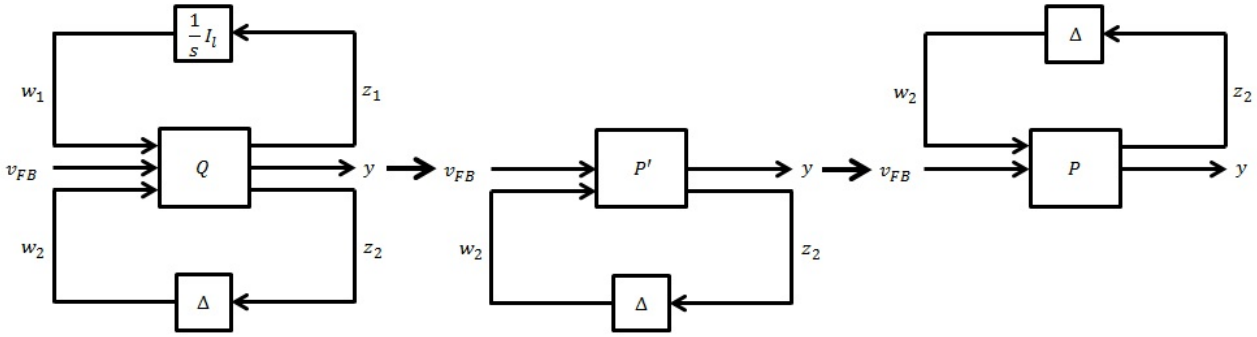

Fig. 2. Block diagram manipulation to obtain generalized plant P.

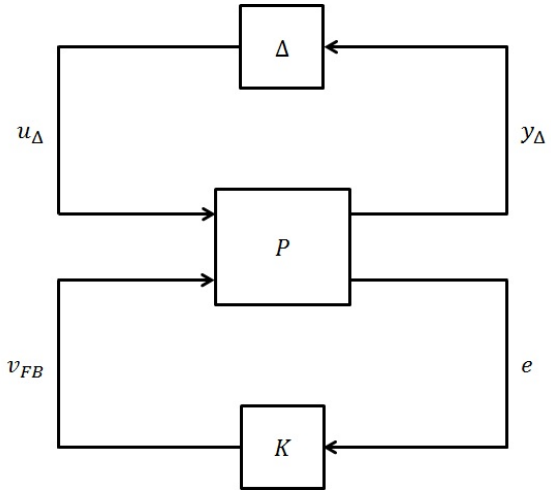

Fig. 3. Model in $\Delta - P - K$ robust control framework.

The representation of the matrix M_a, defined in (21), is equal to the lower LFT

$$\begin{aligned} M_a &= F_l(Q,\Delta) = Q_{11} + Q_{12}\Delta(I_{q_T} - Q_{22}\Delta)^{-1}Q_{21} \\ &= Q_{11} + Q_{12}\Delta Q_{21} \end{aligned} \tag{23}$$

where

$$Q = \begin{bmatrix} Q_{11} & Q_{12} \\ Q_{21} & 0 \end{bmatrix}, \tag{24}$$

$q_T = \sum_{n=1}^{l+1} q_n$ is the total rank of the Δ matrix, and F_l denotes the lower LFT. The block diagram of the system is now drawn as in Figure 2 (left).

The transfer function $G(s)$ of the uncertain state-space model is next expressed as

$$\begin{aligned} G(s) &= F_u\left(M_a, \frac{1}{s}I_l\right) = F_u\left(F_l(Q,\Delta), \frac{1}{s}I_l\right) \\ &= F_l\left(F_u\left(Q, \frac{1}{s}I_l\right), \Delta\right) = F_l(P',\Delta). \end{aligned} \tag{25}$$

For convention purposes, it is necessary to move the uncertainty to create an upper LFT by employing the definition

$$G(s) = F_l(P',\Delta) = F_u(P,\Delta) \tag{26}$$

where

$$P' = \begin{bmatrix} P_{22} & P_{21} \\ P_{12} & P_{11} \end{bmatrix} \quad P = \begin{bmatrix} P_{11} & P_{12} \\ P_{21} & P_{22} \end{bmatrix}. \tag{27}$$

The corresponding block diagram manipulation is shown in Figure 2. Using the partition of the generalized plant $P \in \mathbb{R}^{(q_T+l)\times(q_T+3)}$, defined in (27), the input/output equations of the system are

$$z_2 = P_{11}w_2 + P_{12}v_{FB} \qquad y = P_{21}w_2 + P_{22}v_{FB} \tag{28}$$

where $P_{11} \in \mathbb{R}^{q_T \times q_T}$, $P_{12} \in \mathbb{R}^{q_T \times 3}$, $P_{21} \in \mathbb{R}^{l \times q_T}$, $P_{22} \in \mathbb{R}^{l \times 3}$, $z_2 \in \mathbb{R}^{q_T \times 1}$, $w_2 \in \mathbb{R}^{q_T \times 1}$, $y \in \mathbb{R}^{l \times 1}$, and $v_{FB} \in \mathbb{R}^{3 \times 1}$.

V. Controller Synthesis

The control goal is to design a linear, time invariant, feedback controller K that can robustly stabilize the error dynamics (10) and also keep the tracking error e small in the presence of external disturbances to the system and modeling uncertainties. The feedback system is expressed in the conventional $\Delta - P - K$ robust control framework as shown in Figure 3, where Δ is the uncertainty, $w_2 = u_\Delta$, $z_2 = y_\Delta$, and $y = e$. The control technique employed is this work is the loop-shaping design method developed by Glover and McFarlane [14]. The algorithm computes an optimal H_∞ normalized coprime factor loop-shaping controller K that simultaneously minimizes the following two cost functions

$$\begin{aligned} \gamma &= \min_K \left|\left| \begin{bmatrix} I \\ K \end{bmatrix} (I - G_s K)^{-1} \begin{bmatrix} G_s & I \end{bmatrix} \right|\right|_\infty \\ \gamma &= \min_K \left|\left| \begin{bmatrix} I \\ G_s \end{bmatrix} (I - K G_s)^{-1} \begin{bmatrix} K & I \end{bmatrix} \right|\right|_\infty \end{aligned} \tag{29}$$

where $||\cdot||_\infty$ denotes the H_∞ norm, γ is the H_∞ optimal cost, $G_s = W_{p_2} \times G_{nom} \times W_{p_1}$ is the shaped nominal plant, and W_{p_1} and W_{p_2} are weight functions chosen by the designer. The nominal plant, G_{nom}, is computed via (26) with the uncertainty Δ set to its nominal value of zero. The weight functions are chosen to achieve a desired performance of the closed-loop system and are defined as [15]

$$W_{p_1}(s) = F_1 \frac{\left(s/\sqrt{M_{p_1}} + \omega_{b_1}\right)^2}{\left(s + \omega_{b_1}\sqrt{H_1^*}\right)^2} \quad W_{p_2}(s) = \frac{\left(s/\sqrt{M_{p_2}} + \omega_{b_2}\right)^2}{\left(s + \omega_{b_2}\sqrt{H_2^*}\right)^2} \tag{30}$$

where $F_1 = 1.1$, $M_{p_1} = M_{p_2} = 1$, $H_1^* = H_2^* = 10^{-1}$, $\omega_{b_1} = 1$, and $\omega_{b_2} = 10^{-1}$. The robust feedback controller K found by solving (29) is written in state-space form as

$$\dot{x}_c = A_c x_c + B_c e(t) \qquad v_{FB}(t) = C_c x_c + D_c e(t) \tag{31}$$

where the vector $x_c \in \mathbb{R}^{m \times 1}$ is the internal controller states, $A_c \in \mathbb{R}^{m \times m}$, $B_c \in \mathbb{R}^{m \times l}$, $C_c \in \mathbb{R}^{3 \times m}$, and $D_c \in \mathbb{R}^{3 \times l}$ are the

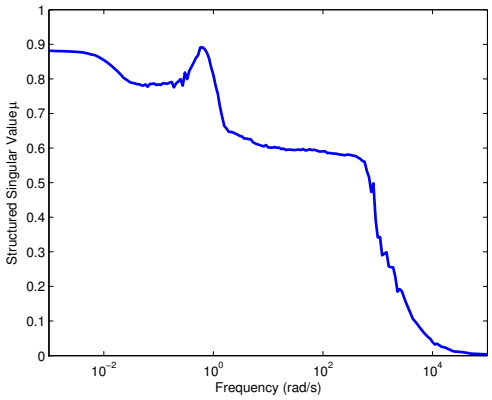

Fig. 4. Structured singular value μ versus frequency.

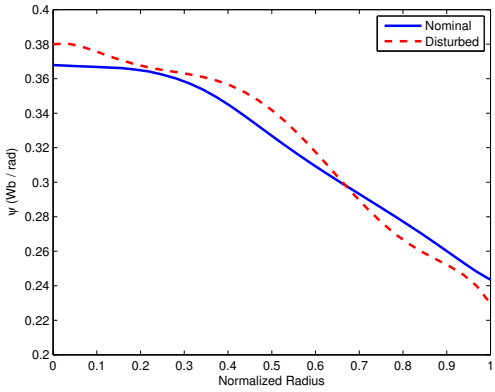

Fig. 5. Poloidal flux $\psi(\hat{\rho})$ at time $t = 0.5$ seconds.

controller system matrices, and m is the number of controller states. The initial controller state vector is $x_c(0) = [0]$.

The structure of the uncertainty in the system transfer function representation (26) is now taken into account to analyze the robust stability of the closed-loop system. To make use of the structured uncertainty, the system is formulated into the $N-\Delta$ structure where $N = F_l(P,K)$. Because the uncertainty has a defined structure, $\Delta = \text{diag}\{\delta_n\}$, we can define the structured singular value μ as

$$\mu\big(N(j\omega)\big) = \frac{1}{\min\{k_m | \det(I - k_m N\Delta) = 0\}}. \qquad (32)$$

The closed-loop system is robustly stable for all allowable perturbations if and only if $\mu\big(N(j\omega)\big) < 1, \forall\omega$ [15]. Figure 4 shows a plot of μ versus frequency, and $\mu < 1, \forall\omega$. Therefore the closed-loop system is robustly stable.

VI. Simulation Study

In this section, we present the simulation results of the combined feedforward [10], [11] + feedback (31) controller. First, because the control inputs $u_1(t)$, $u_2(t)$, and $u_3(t)$ of the magnetic diffusion equation (1) have large order of magnitude differences, the magnetic diffusion equation is normalized. This normalization is accomplished by determining the maximum feedforward values of the three control inputs respectively. The normalization factors are chosen as $u_{1_{norm}} = 4.4(10)^{15}$, $u_{2_{norm}} = 3.3(10)^{-3}$ and $u_{3_{norm}} = 1.3(10)^{6}$. The parameters in the governing PDE (1) are scaled as

$$f_1^s(\hat{\rho}) = u_{1_{norm}} f_1(\hat{\rho}) \quad f_2^s(\hat{\rho}) = u_{2_{norm}} f_2(\hat{\rho}) \quad k_3^s = u_{3_{norm}} k_3 \qquad (33)$$

where $(\cdot)^s$ denotes the scaled quantity. The analysis presented in sections III and IV is then performed to obtain the system transfer function representation (26). The feedback control law (31) is found by solving (29), and the robust stability of the closed-loop system is determined by computing μ.

The magnetic diffusion equation model of the poloidal flux profile time evolution in a tokamak presented in section II is denoted as the nominal plant, and the nominal initial poloidal flux profile $\psi^{nom}(\hat{\rho}, t_i)$ is shown in Figure 5, which is extracted from DIII-D shot #129412. This nominal model and initial condition were used to compute the optimal feedforward control trajectories [10], [11] and to compute the feedback controller (31). The experimental time interval associated with the plasma current ramp-up phase of the discharge is $[t_i, t_{f_{ru}}] = [0.5s, 1.7s]$, and it is the time interval chosen to design the feedback controller.

In normal tokamak operation, it is difficult to achieve a perfect matching of the nominal initial poloidal flux profile. Also, all of the physical phenomena that effect the poloidal flux time evolution in a tokamak are not modeled by the magnetic diffusion equation. This modeling uncertainty will result in an actual poloidal flux profile time evolution that is different from the time evolution predicted by the nominal model. In order to test the combined feedforward + feedback controller through simulation, the initial poloidal flux profile is perturbed, and the nominal electron temperature and the nominal non-inductive current density models are perturbed by 10%. These simulation conditions provide the means to test the combined controller in a realistic tokamak operating scenario. The disturbed initial poloidal flux profile $\psi^{dis}(\hat{\rho}, t_i)$ is shown in Figure 5. A closed-loop simulation, with the perturbed initial flux profile and modified magnetic diffusion equation model is conducted to determine the performance of the closed-loop (feedforward + feedback) controller. The performance is determined based on the ability of the closed-loop controller to recover the desired final time nominal poloidal flux profile $\psi(\hat{\rho}, t_{f_{ru}})$. The nominal system with open-loop (feedforward) control represents the desired poloidal flux profile time evolution.

The ramp-up phase of tokamak discharge ends at an experimental time of $t = 1.7$ seconds, and the flat-top phase begins. Figure 6(a) shows the poloidal flux profile $\psi(\hat{\rho})$ matching comparison at the end of the ramp-up phase, between the nominal system with open-loop control, the disturbed system with closed-loop control, and the disturbed system with open-loop control. The feedback controller is left on for the early flat-top phase $[t_{f_{ru}}, t_{f_{ft}}] = [1.7s, 2.9s]$ of the discharge to determine if the profile matching comparison could be further improved. Figures 6(b) and 6(c) show the poloidal flux profile $\psi(\hat{\rho})$ matching comparison at experimental times of $t = 2.3$ and $t = 2.9$ seconds respectively. As can be seen from the figures, the closed-loop (feedforward + feedback) controller is able to keep the poloidal flux profile closer to the desired nominal profile more effectively than the

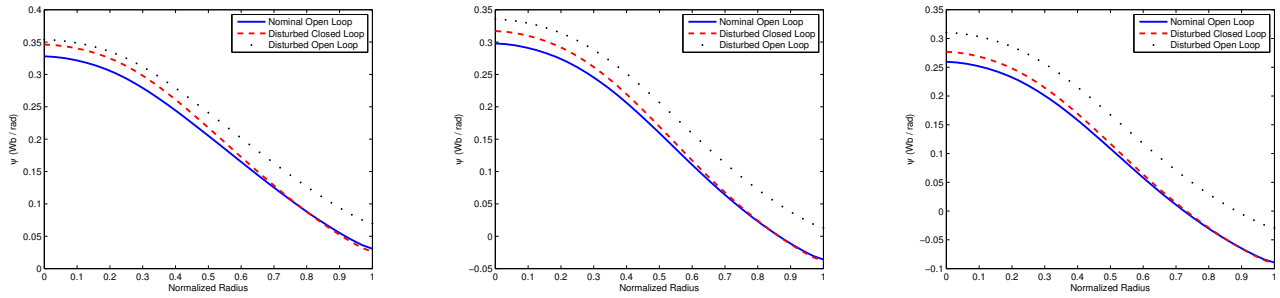

(a) (b) (c)

Fig. 6. (a) Poloidal flux $\psi(\hat{\rho})$ at time $t = 1.7$ seconds, (b) poloidal flux $\psi(\hat{\rho})$ at time $t = 2.3$ seconds, and (c) poloidal flux $\psi(\hat{\rho})$ at time $t = 2.9$ seconds.

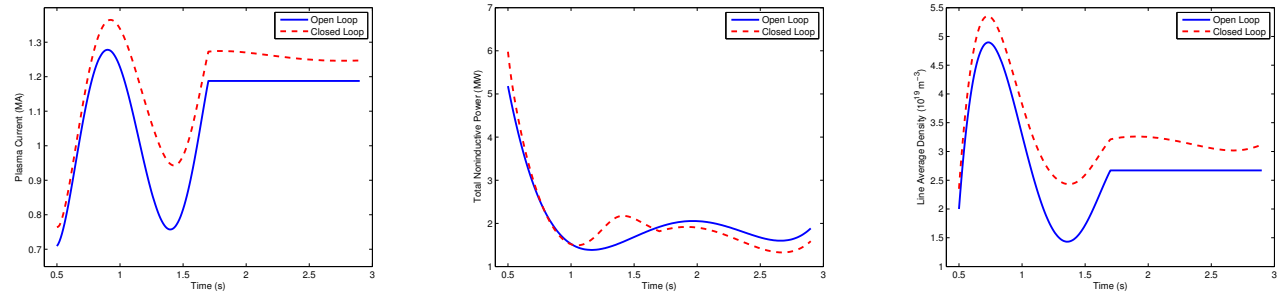

(a) (b) (c)

Fig. 7. Control trajectory comparison: (a) plasma current (MA), (b) total non-inductive power (MW), and (c) line average density (10^{19} m^{-3}).

open-loop (feedforward) controller in the presence of the disturbances. As the simulation progresses into the beginning of the flat-top phase, the error between the disturbed system with open-loop control and the nominal system increases, but the error between the disturbed system with closed-loop control and the nominal system continues to decrease or remains constant. This demonstrates the robust stability provided by the feedback component of the closed-loop controller. A comparison of the open-loop and closed-loop control trajectories for $I(t)$, $P_{tot}(t)$, and $\bar{n}(t)$ is shown in Figure 7. The figure shows that the feedforward control trajectories are modified by the feedback component of the closed-loop controller throughout the simulation to overcome the disturbances generated by the perturbed initial flux profile and the modeling uncertainty.

VII. Conclusions and Future Work

We employed a truncated Taylor series expansion in space to reduce the magnetic diffusion equation model into a finite dimensional system of ordinary differential equations. The reduced-order model was linearized around the optimal feed-forward system trajectories to obtain a linear, time varying model of the tracking error dynamics. The time varying parameters were modeled as an uncertainty, and a feedback controller was synthesized based on the normalized coprime factor loop-shaping technique. The simulation study shows that the proposed feedforward + feedback controller is able to reject disturbances introduced through a perturbed initial flux profile and a modeling uncertainty. Our future work will consist of implementing this advanced, model-based controller in the DIII-D plasma control system, and then of experimentally testing the controller in the DIII-D tokamak.

References

[1] D. Moreau *et al.*, "A Two-time-scale Dynamic-model Approach for Magnetic and Kinetic Profile Control in Advanced Tokamak Scenarios on JET," *Nuclear Fusion*, vol. 48, no. 10, p. 106001, 2008.

[2] L. Laborde *et al.*, "A Model-based Technique for Integrated Real-time Profile Control in the JET Tokamak," *Plasma Physics and Controlled Fusion*, vol. 47, pp. 155–183, 2005.

[3] D. Moreau *et al.*, "Real-time Control of the q-profile in JET for Steady State Advanced Tokamak Operation," *Nuclear Fusion*, vol. 43, pp. 870–882, 2003.

[4] O. Barana *et al.*, "Feedback Control of the Lower Hybrid Power Deposition Profile on Tore Supra," *Plasma Physics and Controlled Fusion*, vol. 49, pp. 947–967, 2007.

[5] T. Wijnands *et al.*, "Feedback Control of the Current Profile on Tore Supra," *Nuclear Fusion*, vol. 37, pp. 777–791, 1997.

[6] T. Suzuki *et al.*, "Recent RF Experiments and Application of RF Waves to Real-Time Control of Safety Factor Profile in JT-60U," in *AIP Conference Proceedings*, 2005, pp. 279–286.

[7] E. Witrant *et al.*, "A Control-oriented model of the Current Profile in Tokamak Plasma," *Plasma Physics and Controlled Fusion*, vol. 49, pp. 1075–1105, 2007.

[8] Y. Ou *et al.*, "Towards Model-Based Current Profile Control at DIII-D," *Fusion Engineering and Design*, vol. 82, pp. 1153–1160, 2007.

[9] J. Ferron *et al.*, "Feedback Control of the Safety Factor Profile Evolution during Formation of an Advanced Tokamak Discharge," *Nuclear Fusion*, vol. 46, no. 10, pp. L13–17, 2006.

[10] C. Xu *et al.*, "Ramp-Up Phase Current Profile Control of Tokamak Plasmas via Nonlinear Programming," *IEEE Transactions on Plasma Science*, vol. 38, pp. 163–173, 2010.

[11] Y. Ou *et al.*, "Design and Simulation of Extremum-Seeking Open-Loop Optimal Control of Current Profile in the DIII-D Tokamak," *Plasma Physics and Controlled Fusion*, vol. 50, p. 115001, 2008.

[12] W. Schiesser, *The Numerical Method of Lines: Integration of Partial Differential Equations*. Academic Press, San Diego, 1991.

[13] A. Packard, "Whats New with μ: Structured Uncertainty in Multivariable Control," Ph.D. dissertation, Univ. of Calif., Berkeley, 1988.

[14] D. McFarlane and K. Glover, "A Loop Shaping Design Procedure using H_∞ Synthesis," *IEEE Transactions on Automatic Control*, vol. 37, no. 6, pp. 759–769, 1992.

[15] S. Skogestad and I. Postlethwaite, *Multivariable Feedback Control Analysis and Design*. John Wiley & Sons Ltd, 2005.